



Cite this: *React. Chem. Eng.*, 2019, 4, 939

On the prevailing reaction pathways during magnesium production *via* carbothermic reduction of magnesium oxide under low pressures†

Adrian Coray and Zoran R. Jovanovic *

In this work we identify the prevailing reaction pathways of carbothermic reduction of MgO for the temperature and pressure ranges of 1375–1450 °C and 1–2 kPa, respectively, and normalized reduction extents of up to 0.4. It has been previously suggested that Mg_(g) is produced by either (i) MgO dissociation forming O₂ as the reaction intermediate or (ii) MgO_(s)–C_(s) boundary reaction producing CO that then reduces MgO while forming CO₂ as the reaction intermediate. Either of the intermediates (O₂ or CO₂) are then consumed by C, which is necessary to sustain further Mg_(g) production. To identify the prevailing pathways, O₂ or CO₂ was co-fed with Ar to sweep reacting MgO–C blends with the intent to shift the equilibrium of one of the suspected Mg_(g)-producing reactions. After accounting for envisaged effects of both the C/MgO ratio in the reacting blends and the CO concentration in the reaction atmosphere, it is demonstrated that Mg_(g) is produced *via* (1) MgO thermal dissociation and (2) MgO reduction with CO that take place in parallel. At 1375 °C and 1400 °C, roughly twice as much Mg_(g) was produced *via* pathway (1) as compared to pathway (2). There is no evidence supporting the relevance of a direct MgO_(s)–C_(s) boundary reaction.

Received 9th November 2018,
Accepted 13th February 2019

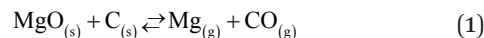
DOI: 10.1039/c8re00295a

rsc.li/reaction-engineering

1 Introduction

The automotive industry has been considering magnesium (Mg) as an attractive substitute for the 50% denser aluminum (Al) to decrease the fuel consumption of vehicles by lowering their weight.^{1–3} Commercially, Mg is produced mainly by the Pidgeon process, which is based on the reduction of magnesium oxide (MgO) by ferrosilicon (Fe_xSi).^{1,3,4} However, compared to the process for making Al this process consumes more than twice the energy (133 *versus* 54 MJ kg^{−1})‡ and releases as much as three times more CO₂ (25.4 *versus* 8.7 kg CO_{2eq} per kg).^{5,6} Therefore, in order to exploit the potential for the fuel efficiency benefit owing to lightweighting of vehicles, the embedded energy content in Mg must be reduced.⁷ One way to achieve this goal is to circumvent the need for the energy-intensive production of ferrosilicon by using carbon (C) as the reducing agent and produce Mg *via* carbothermic reduction (CTR) of MgO.^{2,8,9}

The carbothermic reduction of MgO constitutes a myriad of elementary reaction steps that can be summarized by the following overall reaction (1):^{8–13}



Thermodynamic calculations indicate that the temperature required for the forward reaction (1) to proceed is dependent on the partial pressures of the products.^{8,9,13,14} Reducing these from 50 to 0.5 kPa decreases the onset temperature of the forward reaction from ~1750 °C to ~1350 °C, thereby reducing heat losses and the energy required to preheat the reactants. In addition, it has been demonstrated that lower CO partial pressures drastically decrease the severity of the reverse reaction (1), which takes place during cooling of the product mixture.^{14,15} These benefits thus present a strong incentive for investigating the CTR under vacuum, as they may compensate for the additional pumping work required to maintain low reaction pressures.

In spite of the extensive research dedicated to understanding the constituent steps of reaction (1),^{14,16,17} at present there is no consensus on the prevailing mechanism of the carbothermic reduction. The reported findings gravitate around two hypotheses. The first one has been advocated by Komarek *et al.*¹⁶ who have proposed that MgO first dissociates into Mg_(g) and O and that the latter then diffuses to the C-surface where it reacts to form CO. The authors have not commented on excluding the recombination of the atomic oxygen from consideration, which is believed to be very fast at the temperatures of interest. This recombination

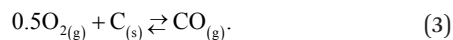
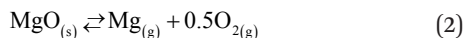
Department of Mechanical and Process Engineering, ETH Zürich, 8092 Zürich, Switzerland. E-mail: zjovanovic@ethz.ch

† Electronic supplementary information (ESI) available. See DOI: 10.1039/c8re00295a

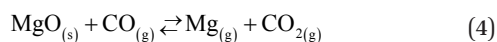
‡ Exclusive upstream processes.



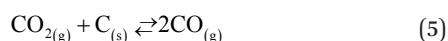
transforms their proposed mechanism into its equivalent, summarized as follows:



On the other hand, Rongti *et al.*¹⁷ and Chubukov *et al.*¹⁴ have advocated the mechanism according to which MgO is directly reduced by both C and CO. Specifically, the Mg_(g) production is initiated by the MgO_(s)-C_(s) boundary reaction (1) that prevails up to MgO conversions of $X_{\text{MgO}} = 0.2$ (ref. 14)–0.25 (ref. 17). At conversions higher than these, the MgO is reduced mainly by CO



as the contribution of the MgO_(s)-C_(s) boundary reaction to the total Mg_(g) production decreases because of a loss in the C_(s)/MgO_(s) contact that has been attributed to (i) the decrease in the surface areas of the reactants due to CTR itself,¹⁴ (ii) sintering of MgO,¹⁴ or (iii) densification of MgO.¹⁷ The production of Mg_(g) by reaction (4) is sustained by oxidation of C with CO₂



which not only removes CO₂ from the reaction site but also replenishes the reducing agent CO.

Experimental evidence supporting the significance of reaction (4) has been provided by Rongti *et al.*¹⁷ and Chubukov *et al.*¹⁴ Rongti *et al.*¹⁷ investigated the effect of CO concentration on the kinetics of MgO reduction by graphite. Exploiting non-isothermal thermogravimetry at atmospheric pressure, these authors have observed an increase in the Mg_(g) production rate upon switching the reaction atmosphere from pure Ar to CO-Ar mixtures containing 10 or 20% CO. The authors have attributed this observation to the facilitating effect of an increase in the CO concentration on reaction (4). However, the reduction in pure CO was much slower than in pure Ar which has been attributed to the suppressing effect of high CO concentrations on the removal of CO₂ from the reduction site *via* reaction (5). Chubukov *et al.*¹⁴ studied the kinetics of MgO reduction with carbon black under isothermal/isobaric conditions at temperatures and total pressures in the range of 1350–1650 °C and 0.1–100 kPa, respectively. Depending on the MgO conversion, these authors observed a dual effect of decreasing the total pressure on the Mg_(g) production rate that they explained as follows:

1. At $X_{\text{MgO}} < 0.2$, a decrease in the total pressure increases the reaction rate, which was attributed to favoring the MgO_(s)-C_(s) boundary reaction (1).

2. At $X_{\text{MgO}} > 0.35$, reducing the total pressure decreases the reaction rate, which was attributed to higher removal rates of CO and CO₂ from the reaction zone. It, however, remains unclear why an increased removal rate of CO₂ from the reaction zone would decrease the rate of CTR as it should actually favor reaction (4).

In spite of the limited experimental evidence supporting the contribution of the reaction pathway comprising reaction steps 4 and 5,^{14,17} the current literature^{12,14,17–20} neither conclusively proves its prevalence in the overall reaction nor justifies ruling out the contribution of the alternative pathway comprising reactions (2) and (3). The objective of this work is to reconcile previously reported findings and conclusively discriminate prevailing reaction pathways that dominate the Mg_(g) production.

2 Methodology

2.1 The principle

The candidates for the prevailing reaction pathways discussed in the previous section may be distinguished by the gaseous intermediates they involve:

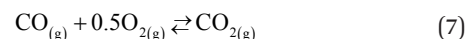
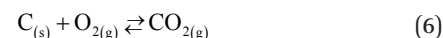
I. If Mg_(g) is produced by the thermal dissociation of MgO *via* reaction (2), O₂ acts as the key intermediate.

II. If Mg_(g) is produced by the MgO reduction with CO *via* reaction (4), CO₂ acts as the key intermediate.

III. If Mg_(g) is produced by the MgO_(s)-C_(s) boundary reaction (1), no gaseous intermediate is formed.

It should be noted that in cases I and II involving the formation of gaseous intermediates the Mg_(g) production is sustained by the removal of those intermediates from the reaction site by the reactions with C. This means that the Mg_(g) production should be suppressed if the partial pressures of those intermediates were increased above the values shown in section S1 of the ESI,[†] thereby shifting the equilibria of both reactions (2) and (4) towards the reactants. Therefore, the prevailing reaction pathway(s) may be discriminated by comparing the extents of CTR in the case when a reacting C/MgO blend is swept with an O₂-Ar mixture and a CO₂-Ar mixture with the extents of CTR in the cases when the same blend is reacted without adding any oxidants to the sweep and then implementing the logic outlined in Fig. 1 as follows:

- The MgO dissociation is the prevailing pathway if the CTR is suppressed with the O₂-Ar but not with the CO₂-Ar sweep.
- The MgO reduction with CO is the prevailing pathway if the CTR is suppressed with the CO₂-Ar but not with the O₂-Ar sweep.
- The MgO_(s)-C_(s) boundary reaction is the prevailing pathway if the CTR remains unaffected by the presence of either O₂ or CO₂ in the sweep gas.
- If the CTR were suppressed with both the O₂-Ar and the CO₂-Ar sweeps, it would appear that both MgO dissociation and MgO reduction with CO pertain to the Mg production. However, this conclusion may be confounded by an extra CO₂ production under the O₂-Ar sweep *via* reactions



that may increase the ratio $p'_{\text{CO}_2}/p'_{\text{CO}}$, thereby shifting the equilibrium of reaction (4) towards the reactants. It would therefore be unclear whether the suppression of the CTR under the O₂-Ar



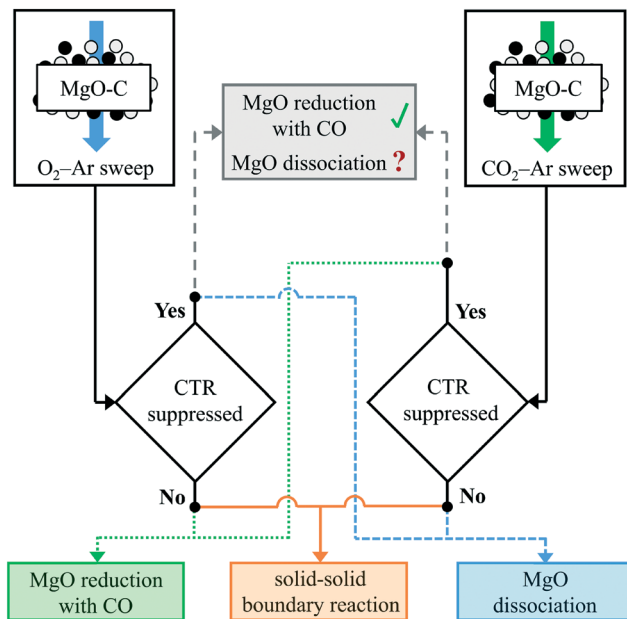


Fig. 1 The logic for discriminating the prevailing reaction pathway. Note: the question mark for the MgO dissociation pathway in the top middle box implies the need for consideration of the effective species partial pressures in the reaction atmosphere under the O_2 -Ar sweep.

sweep was the result of the equilibrium shifts of reaction (2) or (4) without information about the effective partial pressures of CO_2 , CO, and $Mg_{(g)}$ in the reaction atmosphere.

It should be noted, however, that compared to the reference cases in which no oxidant is added into the gas sweeping a reacting C/MgO blend, the addition of O_2 or CO_2 into the sweep gas introduces two side effects: (i) it increases consumption of C *via* reactions (3), (5), and (6) and (ii) it affects the effective p'_{CO} in the reacting atmosphere because of the additional CO production *via* reactions (3) and (5) and/or its consumption *via* reaction (7). Previous research has suggested that the rate of CTR decreases with a decrease in C/MgO molar ratio^{11,17} while it may either increase or decrease with an increase in p'_{CO} .^{14,17} In addition, it has also been reported that the rate of CTR decreases with time, which has been attributed to a gradual sintering of MgO particles¹⁴ that may proceed at different rates depending on the reaction atmosphere. Therefore, the addition of either of the suspected intermediates into the sweep gas may affect the $Mg_{(g)}$ production not only because of favoring reverse reaction (2) or (4) but also because of (i) the differences in the effective C/MgO ratios and CO partial pressures and (ii) the atmosphere-assisted sintering of the MgO particles.

2.2 Accounting for the effects of side reactions

Fig. 2 qualitatively illustrates the expected temporal amounts of C in a MgO-C blend (top) and CO partial pressures over the same blend (bottom) when the blend is swept with Ar (Fig. 2a) or Ar diluted with a suspected intermediate (Fig. 2b) while subjected to a temperature program indicated by the

dotted lines (middle) comprising three stages: (i) heat up ramp from ambient to a setpoint reaction temperature (T_{sp}), (ii) hold at T_{sp} , and (iii) cool-down ramp from T_{sp} to the ambient temperature. As shown in the top part of Fig. 2a, when pure Ar is used as the sweep gas the amount of C remains at its initial value N_C^0 until $t = \tau_1$ when the blend reaches the onset temperature of CTR (T_1), thus $N_C^0 = N_C(\tau_1)$ for $t < \tau_1$. With the further progress of the temperature program, C is consumed solely by CTR until $t = \tau_{II}$ when the temperature drops below T_1 during the cool-down ramp. Therefore the amount of C remains at $N_C(\tau_f)$ for $t \geq \tau_{II}$. However, if either O_2 or CO_2 is added to the sweep gas, it starts oxidizing C at a temperature T_{ox} that is generally lower than T_1 . This is illustrated by the top part of Fig. 2b illustrating that within the time interval $\tau_{ox} \leq t < \tau_1$ C is consumed by the reaction with the added oxidant before T_1 is reached, implying that the amount of C at the onset of CTR ($N_C(\tau_1)_{lim}$) is lower than the initial amount ($N_C^0_{lim}$). After this point of time, *i.e.*, $\tau_1 \leq t \leq \tau_{II}$, C is consumed both by the reaction with the added oxidant and by CTR until the temperature drops below T_1 . As the temperature decreases from T_1 to T_{ox} ($\tau_{II} < t \leq \tau_f$) the amount of C continues to decrease because of the reaction with the oxidant to eventually stabilize at ($N_C(\tau_f)_{lim}$) for $t \geq \tau_f$. Due to likely high rates of the oxidation reactions at the temperatures in question, the consumption of C by the added oxidant is expected to be mass-transfer limited, thereby occurring at a constant rate owing to a constant gas velocity and an insignificantly decreasing particle size.²¹ Accordingly, the amount of C that would be observed in the absence of CTR, *i.e.* in the absence of MgO, is designated by the straight dashed line in the top sketch of Fig. 2b ($\tilde{N}_C(t)_{lim}$). Therefore, the amount of C consumed by CTR only is represented by $\tilde{N}_C(\tau_f)_{lim} - N_C(\tau_f)_{lim}$. The analogous description applies for the discussion of temporal CO partial pressures illustrated in the bottom parts of Fig. 2. Again, the constant partial pressure of CO that would be observed in the absence of CTR ($\tilde{p}_{CO,lim}$) stems from the assumption that the consumption of C by the added intermediate is mass-transfer limited.

In general, the rates of C consumption and the resulting CO production by the side reactions of the suspected intermediates with C are specific to the oxidant added to the sweep gas. The dependence of these rates on the total sweep gas flow rate and/or the partial pressure of the oxidants can be assessed through a series of tests with pure C and/or C-(inert solid) blends swept with O_2 -Ar and CO_2 -Ar mixtures. The equal amounts of C available for CTR regardless of which oxidant is fed with the sweep, *i.e.*,

$$\begin{aligned} \tilde{N}_C(\tau_1)_{O_2} &= \tilde{N}_C(\tau_1)_{CO_2}, \\ \tilde{N}_C(\tau_f)_{O_2} &= \tilde{N}_C(\tau_f)_{CO_2}, \end{aligned} \quad (8)$$

can then be ensured by manipulating one or more of the following parameters: (i) the initial amounts of C ($N_C^0|_{O_2}$ and $N_C^0|_{CO_2}$), (ii) the flow rates of the O_2 -Ar and



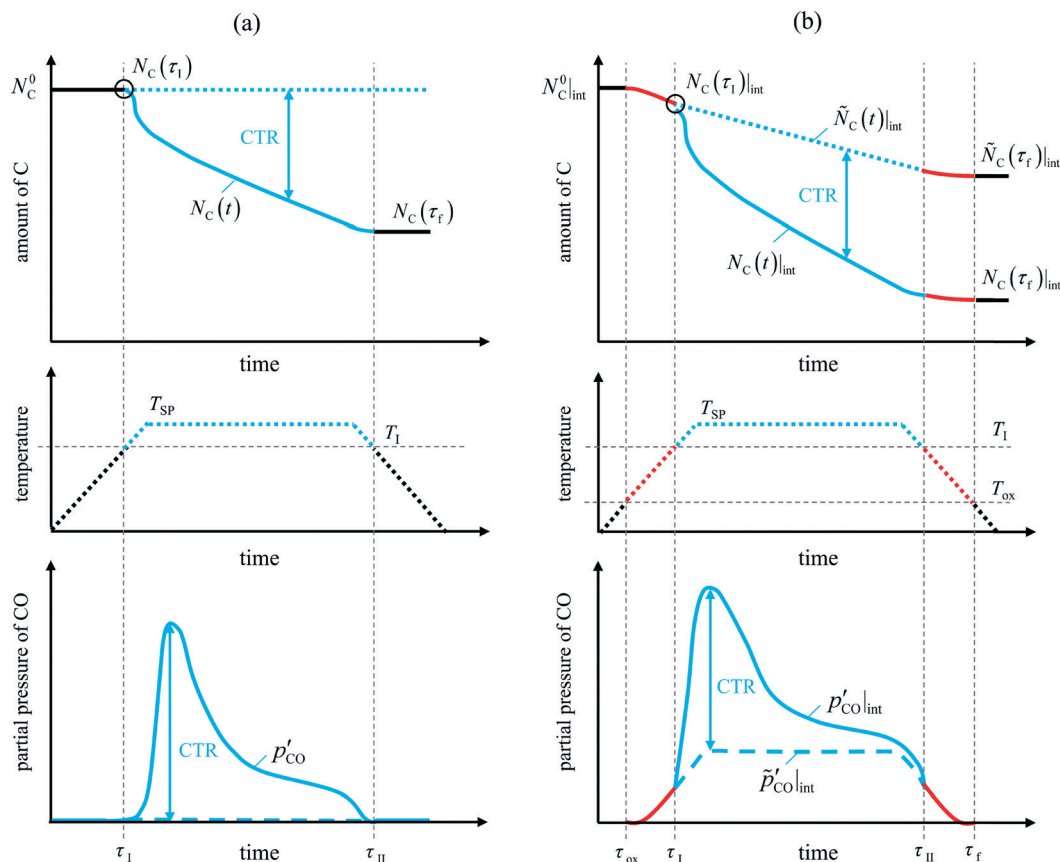


Fig. 2 Qualitative temporal amounts of C in a reacting MgO–C blend (top) and CO partial pressures over the same blend (bottom) when it is swept with (a) Ar and (b) Ar diluted with O₂ or CO₂ as the suspected intermediate (abbreviated as “int”) under the temperature program indicated by the dotted lines (middle). The dashed lines indicate the amounts of C and the partial pressures of CO that would be observed in the absence of the carbothermal reduction.

CO₂–Ar sweep gas mixtures, and (iii) the partial pressures of O₂ and CO₂ in the sweep gas mixtures.

However, even when the feed rates and compositions of the O₂–Ar and the CO₂–Ar sweep gas mixtures are adjusted to ensure the same consumption rates of C, the corresponding CO production rates are different because the oxidation of C with CO₂ produces twice as much CO per mole of C. This results in $\tilde{p}'_{\text{CO}}|_{\text{CO}_2} > \tilde{p}'_{\text{CO}}|_{\text{O}_2}$, which may affect the extent of CTR through the effect of the CO partial pressure on the onset temperature of CTR and/or its rate. Moreover, even though satisfying the equation set (8) ensures that the amounts of C available for CTR under the O₂–Ar and CO₂–Ar sweeps are roughly the same at all times, the amount of C decreases with time faster in these cases than if no oxidant is added to the sweep. Therefore, the presence of oxidants in the sweep may result in a lower extent of the CTR merely because of a lower amount of C available for CTR but not because of suppressing forward reactions (2) and/or (4). To account for the effects of the differences in both the amounts of C available for CTR and the effective CO partial pressures, one thus needs to establish a reference for comparing the extents of CTR obtained under sweep gas mixtures containing O₂ or CO₂ with those measured in the absence of either of the oxidants in the sweep. Such a reference range of the extents may

be determined by using the initial amounts of C set at

$$N_{\text{C}}^0|_{\text{high}} = \tilde{N}_{\text{C}}(\tau_1) \quad (9)$$

$$N_{\text{C}}^0|_{\text{low}} = \tilde{N}_{\text{C}}(\tau_f) \quad (10)$$

to react the same amount of MgO under (i) an Ar sweep and (ii) the CO–Ar sweep having the CO partial pressure in the sweep adjusted at $\tilde{p}'_{\text{CO}}|_{\text{CO}_2}$. This choice of the reaction conditions encompasses the expected effects of the extra consumption of C by the oxidants added to the sweep on the C/MgO ratios and CO partial pressures during the CTR. The pertinent reaction pathway(s) may then be conclusively identified if adding an oxidant to the sweep (i) has no effect on the extent of CTR or (ii) it results in a CTR extent that is below the reference range of the CTR extents. If, however, adding an oxidant to the sweep suppresses the Mg production but the corresponding CTR extent is higher than that obtained with no oxidant in the sweep and with $N_{\text{C}}^0|_{\text{low}}$, the decision cannot be made without considering the effective species partial pressures in the reaction atmosphere and/or the effect of the initial C/MgO ratio on the extent of CTR.



3 Experimental

3.1 Program

The methodology presented in the previous section was implemented through the experimental program comprising three phases as outlined in Table S1 of section S2 of the ESI.† The first phase involves experiments exploiting a standard temperature program under an O₂-Ar sweep having the total inlet molar rate and composition set at $\dot{n}^0_{\text{O}_2}$ and $y^0_{\text{O}_2}$, respectively. It starts with comparison experiment #1 which represents the reaction of N^0_{MgO} moles of MgO blended with $N^0_{\text{C}|_{\text{O}_2}}$ moles of C to determine temporal amounts of the residual carbon in the blend ($N_{\text{C}}(t)|_{\text{O}_2}$) indicated by the solid line in the top sketch of Fig. 2b. In the next step of this phase, the same initial amount of C ($N^0_{\text{C}|_{\text{O}_2}}$) was oxidized under the same sweep gas mixture in the absence of MgO to quantify the C consumption in the absence of CTR, *i.e.*, to determine the values of $\tilde{N}_{\text{C}}(t)|_{\text{O}_2}$ indicated by the dashed line in the top sketch of Fig. 2b. With $\tilde{N}_{\text{C}}(t)|_{\text{O}_2}$ and $N^0_{\text{C}|_{\text{O}_2}}$ at hand, one can determine τ_1 and τ_f and, therefore, $\tilde{N}_{\text{C}}(\tau_1)|_{\text{O}_2}$ and $\tilde{N}_{\text{C}}(\tau_f)|_{\text{O}_2}$, as well as the extent of CTR during comparison experiment #1.

Phase 2 repeats the same steps of phase 1 under the standard $N^0_{\text{C}|_{\text{CO}_2}}$, $\dot{n}^0_{\text{CO}_2}$, and $y^0_{\text{CO}_2}$ that ensures the same C consumption in the absence of MgO, as observed in phase 1 (*i.e.*, $\tilde{N}_{\text{C}}(t)|_{\text{CO}_2} = \tilde{N}_{\text{C}}(t)|_{\text{O}_2}$ for $t \geq \tau_1$). The reaction of N^0_{MgO} moles of MgO blended with $N^0_{\text{C}|_{\text{CO}_2}}$ moles of C under the CO₂-Ar sweep gas mixture having the molar rate and CO₂ composition adjusted to satisfy the equalities imposed by eqn (8) represents comparison experiment #2.

Phase 3 involves the reference CTR experiments performed under the standard temperature program in the absence of either O₂ or CO₂ in the sweep. The reacting blends comprised N^0_{MgO} moles of MgO and C in the amounts set according to eqns (9) and (10), with $\tilde{N}_{\text{C}}(\tau_1)$ and $\tilde{N}_{\text{C}}(\tau_f)$ determined in phases 1 and 2. Each of these blends is then reacted under both (i) an Ar sweep and (ii) the CO-Ar sweep having the flow rate and composition adjusted to ensure that the CO partial pressures during the experiments resemble those observed during comparison experiment #2 ($p'_{\text{CO}|_{\text{CO}_2}}$).

The conclusive discrimination among the reaction pathways under consideration is based on establishing that the extent of CTR observed in the comparison experiments (#1 and/or #2) is either (i) unaffected by the presence of the oxidants in the sweep or (ii) lower than the lowest extent of the CTR observed in the reference experiments of phase 3. The former would imply the relevance of the MgO_(s)-C_(s) boundary reaction while the latter would point to reactions (2) and/or (4) as the prevailing pathway(s).

3.2 Materials

Table 1 lists the sources, specific surface areas (Micromeritics TriStar 3000 N₂ adsorption analyzer), volume-based mean particle sizes (HORIBA LA-950 laser scattering analyzer), and

impurities contained in the as-received solid raw materials used in this study: MgO and C as reactants and Al₂O₃ as the inert diluent for the C oxidation experiments in the absence of MgO. The discrepancy between the ratios of the BET areas and the mean particle sizes of MgO and C implies that these materials were either highly porous or that they comprised agglomerates of finer particles.

MgO and Al₂O₃ powders contained H₂O and CO₂ as impurities adsorbed from the surroundings. The MgO powder additionally contained both of these impurities chemically bonded in the forms of Mg(OH)₂ and MgCO₃. The as-received charcoal contained moisture, volatile matter, and ash. The weight fractions of the impurities in the as-received MgO and Al₂O₃ powders ($w^{\text{MgO}}_{\text{imp}}$ and $w^{\text{Al}_2\text{O}_3}_{\text{imp}}$, respectively) and charcoal ($w^{\text{C}}_{\text{H}_2\text{O}}$, w^{C}_{vm} , and $w^{\text{C}}_{\text{ash}}$) were determined as described in section S3 of the ESI.†

3.3 Apparatus

Fig. 3 shows a schematic of the experimental apparatus. The reactant bed ② (a MgO-C blend, an Al₂O₃-C blend, or C alone) was placed into the assembly shown in more detail on the left side of the figure. The reactant bed was poured over the graphite felt (Sigratherm® GFA5) ④ protected with a C layer of $m^*_\text{C} = 0.23$ g ③ to prevent the infiltration of MgO into the felt, thereby allowing the complete recovery of the residual MgO after the reaction. Seven Al₂O₃ tubes (Ø10 × 2 mm, $l = 10$ mm) ⑤ separated the felt bottom from the support ⑥ (Schupp Ceramics, Ultraboard, mullite fibers, Ø58 mm, $l = 20$ mm) in order to prevent a reaction of the SiO₂ from the mullite support with the graphite felt. Seven boreholes (Ø4 mm) in the support allowed the removal of sweep and product gases. The packed bed assembly was placed into a reactor tube ⑦ (Al₂O₃, Ø70 × 5 mm, $l = 1200$ mm) and held in place at the location of the hot zone by five support tubes ⑧ (Al₂O₃, Ø58 × 5 mm, $l = 100$ mm). Heat was provided by an electrically heated tube furnace ⑨ (Carbolite STF 16-450) equipped with an R-type thermocouple ⑩ measuring the temperature in the furnace chamber at the height of the hot zone (the location is indicated by a dot in Fig. 3). The part of the reactor tube below the furnace was cooled by surrounding air *via* natural convection and provided a cooling zone for precipitating the Mg_(g) product. Sweep gas flow rates were controlled by calibrated mass flow controllers ⑪ and ⑫ (Bronkhorst EL-Flow Select series). The low-pressure environment was provided by a vacuum pump ⑬ (Adixen ACP15) protected by a particle filter ⑭ (Whatman, GF/F grade glass fiber filter). The pressure inside the reactor tube was monitored using a pressure sensor ⑯ (Kistler Instrumente AG, type 4045A1) positioned in the cold zone above the furnace and controlled *via* a globe valve ⑰ positioned in front of the vacuum pump. An overpressure relief valve ⑱ was set at 30 kPa overpressure relative to ambient pressure. The product gas composition was measured every 65 seconds using a gas chromatograph ⑲ (Agilent M200).



Table 1 Properties of the starting solid materials.

Material	Source	BET surface area (m ² g ⁻¹)	\bar{d} (μm)	Impurities	
				Type	Wt%
MgO	Sigma-Aldrich, # 342793	141 ± 1	5.2	H ₂ O + CO ₂	5.5
C	Fluka analytical, # 05120	680 ± 20	37	H ₂ O	1.6
				Volatiles	2.4
				Ash	4.1
Al ₂ O ₃	Sigma-Aldrich, # 265497	—	10 ^a	H ₂ O + CO ₂	0.1

^a As reported by the manufacturer.

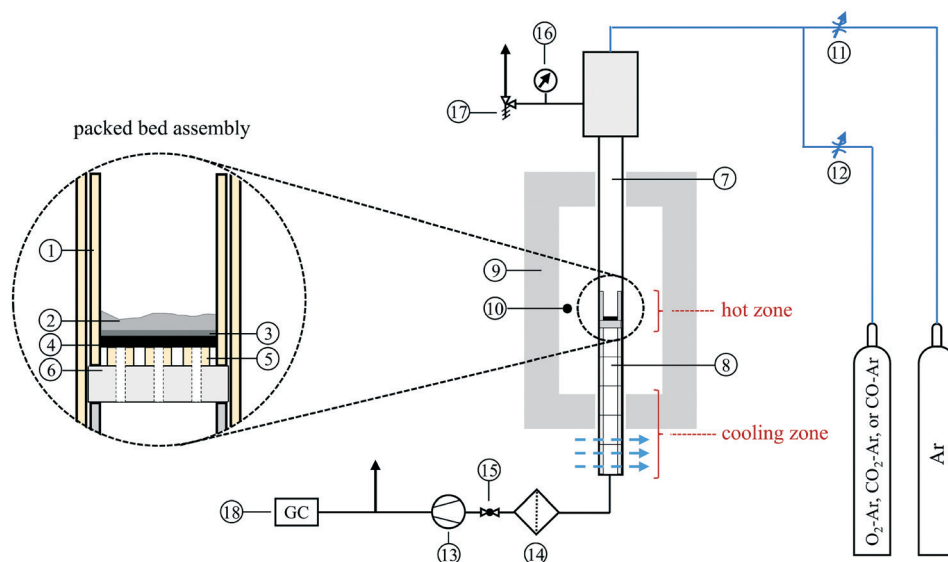


Fig. 3 Schematic of the experimental apparatus with the packed bed assembly situated in the hot zone. The components of the apparatus are the following: ① alumina assembly wall, ② reactant bed, ③ extra C layer, ④ graphite felt, ⑤ alumina separator tubes, ⑥ mullite packed bed support, ⑦ alumina reactor tube, ⑧ alumina support tubes, ⑨ furnace, ⑩ thermocouple, ⑪ mass-flow controller MFC 1, ⑫ mass-flow controller MFC 2, ⑬ vacuum pump, ⑭ particle filter, ⑮ globe valve, ⑯ pressure sensor, ⑰ overpressure relief valve, and ⑱ gas chromatograph.

3.4 Procedure

The MgO-C blends were prepared by stirring m_1^0 grams of as-received MgO powder and m_2^0 grams of as-received charcoal powder with a spatula in a pill glass and occasionally breaking agglomerates until the blends appeared homogeneous. To investigate the reaction of C with O₂ added to the sweep gas, MgO was substituted with m_3^0 grams of as-received Al₂O₃ powder that does not react with C within the pressure and temperature ranges investigated.²² The effective amounts of the MgO, Al₂O₃ and C in the blends (m_{MgO}^0 , $m_{\text{Al}_2\text{O}_3}^0$ and m_{C}^0 , respectively) were calculated as

$$\begin{aligned} m_{\text{MgO}}^0 &= m_1^0 (1 - w_{\text{imp}}^{\text{MgO}}) \\ m_{\text{Al}_2\text{O}_3}^0 &= m_1^0 (1 - w_{\text{imp}}^{\text{Al}_2\text{O}_3}) \\ m_{\text{C}}^0 &= m_2^0 (1 - w_{\text{H}_2\text{O}}^{\text{C}} - w_{\text{vm}}^{\text{C}} - w_{\text{ash}}^{\text{C}}) \end{aligned} \quad (11)$$

The reaction of C with CO₂ added to the sweep gas was investigated using m_2^0 grams of as-received charcoal powder without diluting it with Al₂O₃.

The reactant beds (MgO-C, Al₂O₃-C, or C alone) were poured into the packed bed assembly after which the apparatus was sealed and the vacuum pump was started. Then, the globe valve in front of the vacuum pump was opened and the total pressure inside the reactor was reduced to 0.8–1.9 kPa under 0.16–0.39 L_N min⁻¹ of Ar sweep (Messer 4.6). After pressure equilibration, the furnace was heated under a continuing Ar flow to 1000 °C at a 20 °C min⁻¹ ramp rate and held at 1000 °C for 15 minutes to ensure the complete dissociation of Mg(OH)₂ and MgCO₃ contained in the starting MgO and the evaporation of volatile matter contained in the starting charcoal. In some experiments, the gas flow was then switched to one of the bottled gas mixtures – 5% O₂-Ar (Messer 5.0), 5% CO₂-Ar (Messer 4.8), or 5% CO-Ar (Messer 4.7) flowing at rates in the range of 0.16–0.39 L_N min⁻¹ which resulted in a total pressure of 0.8–1.9 kPa and therefore initial partial pressures of O₂, CO₂ and CO of 40–95 Pa. The furnace was then ramped at 20 °C min⁻¹ to the desired setpoint temperature (T_{sp}) of 1375, 1400 or 1450 °C and held there for 30 minutes, after which the furnace was shut off and



Table 2 Extents of the reactions (i) and (j) taking place (a) in the hot zone (ξ_i) and (b) in the cooling zone (φ_j) when C is swept with O₂-Ar and CO₂-Ar mixtures in the absence of MgO. Note: the extent $\varphi_5^* \geq 0$ refers to the extent of the reverse reaction (5).

C source/sink	Reactions		Phase 1	Phase 2
	Extent	Stoichiometry	O ₂ -Ar	CO ₂ -Ar
Hot zone Consumed by the oxidant added to the sweep	ξ_6	$C_{(s)} + O_{2(g)} \rightleftharpoons CO_{2(g)}$	✓	✗
	ξ_5	$C_{(s)} + CO_{2(g)} \rightleftharpoons 2CO_{(g)}$	✓	✓
Cooling zone Deposited on the column wall	φ_5^*	$2CO_{(g)} \rightleftharpoons C_{(s)} + CO_{2(g)}$	✓	✓

allowed to cool off. When a gas mixture was used as the sweep, it was replaced by Ar when the furnace temperature reached 1250 °C.

A possible deposition of C in the cooling zone *via* reverse Boudouard reaction (5)²³ was tested by feeding a 5% CO-Ar mixture into the empty reactor maintained at 1450 °C under a CO partial pressure of ~95 Pa and measuring the amount of produced CO₂ in the product gas.

3.5 Calculations

3.5.1 Consumption of C and net generation of CO owing to O₂ and CO₂ added to the sweep. The removal of C by the oxidants co-fed with the sweep was quantified exploiting the experiments performed in the absence of MgO based on the reactions listed in Table 2 and the corresponding C balance equations listed in Table 3. The molar extents of reactions occurring in the hot zone (i) and the cooling zone (j) are designated ξ_i and φ_j , respectively. The extent φ_5^* refers to the extent of the reverse reaction (5), *i.e.*, $\varphi_5^* = -\varphi_5$.

$\tilde{N}_C(\tau_i)$ and $\tilde{N}_C(\tau_f)$ (see Fig. 2) were estimated combining balance eqns (12), (14), and (16) for the O₂-Ar sweep and eqns (13) and (15) for the CO₂-Ar sweep as

$$\tilde{N}_C(\tau_i)|_{O_2} = [N_C^0 - N_{CO}(\tau_i) - N_{CO_2}(\tau_i) - \varphi_5^*(\tau_i)]|_{O_2} \quad \text{with } i = I, f \quad (18)$$

$$\tilde{N}_C(\tau_i)|_{CO_2} = [N_C^0 - 0.5N_{CO}(\tau_i) - \varphi_5^*(\tau_i)]|_{CO_2} \quad \text{with } i = I, f. \quad (19)$$

In eqns (18) and (19), $N_i(\tau)$ represents the total molar amount of species *i* entrained with the product gas up to the point of time τ calculated as

$$N_i(\tau) = \int_{\tau_{\text{ox}}}^{\tau} \dot{n}_i(t) dt \quad (20)$$

where the temporal molar flow rate of species *i* in the product gas was determined as

$$\dot{n}_i(t) = y_i(t) \dot{n}(t) \quad (21)$$

with $y_i(t)$ and $\dot{n}(t)$ representing the temporal mole fractions of species *i* determined by gas chromatography and the temporal total molar rates of the product gas, respectively. The latter was calculated as

$$\dot{n}(t) = \frac{\dot{n}_{Ar}(t)}{y_{Ar}(t)} \quad (22)$$

with

$$y_{Ar}(t) = 1 - y_{O_2}(t) - y_{CO}(t) - y_{CO_2}(t) \quad (23)$$

and

$$\dot{n}_{Ar}(t) = y_{Ar}^0 \dot{n}^0(t) \quad (24)$$

where y_{Ar}^0 represents the mole fraction of Ar in the inlet sweep gas mixture and $\dot{n}^0(t)$ is the total molar flow rate of the sweep gas

$$\dot{n}^0(t) = \frac{p_N \dot{V}_N^0(t)}{R T_N} \quad (25)$$

based on the total volumetric inlet flow rate of the sweep gas $\dot{V}_N^0(t)$ standardized with a flow definer (MesaLabs, Bios DryCal Definer 220) at $p_N = 101.3$ kPa and $T_N = 0$ °C for a given output to the mass-flow controller MFC 2.

The only remaining variables needed to calculate the temporal amounts of carbon *via* eqns (18) and (19) are the extents of Boudouard reaction (5) (φ_5^*). As these extents scale with the CO concentration in the cooling zone, they were evaluated by

Table 3 Species material balance equations for the reactions of C with O₂ or CO₂ added to the sweep gas in the absence of MgO.

Amount of C		Phase 1: O ₂ -Ar	Phase 2: CO ₂ -Ar
Remained in the hot zone	N_C	$N_C^0 - \xi_6 - \xi_5$ (12)	$N_C^0 - \xi_5$ (13)
Removed as CO and CO ₂ in the product gas	N_{CO}	$2\xi_5 - 2\varphi_5^*$ (14)	$2\xi_5 - 2\varphi_5^*$ (15)
	N_{CO_2}	$\xi_6 - \xi_5 + \varphi_5^*$ (16)	$N_{CO_2, fed} - \xi_6 + \varphi_5^*$ (17)



flowing a pilot CO–Ar stream through the setup kept under typical reaction conditions. This evaluation demonstrated the absence of CO₂ in the effluent at a CO partial pressure of 95 Pa, thereby allowing to consider that $\varphi_5^* = 0$ for $p_{\text{CO}} \leq 95$ Pa.

Under the CO₂–Ar sweep, temporal partial pressures of CO in the hot zone expected in the absence of CTR were approximated by the values that were observed during the C oxidation experiments in the absence of MgO as

$$\tilde{p}'_{\text{CO}}|_{\text{CO}_2} = [\tilde{y}_{\text{CO}}(t)\tilde{p}'_{\text{tot}}(t)]|_{\text{CO}_2} \quad (26)$$

Under the O₂–Ar sweep, however, the outlet rate of CO may not be representative of the CO rate coming from the hot zone because of CO oxidation *via* reaction (7) that may have proceeded in the cooling zone. However, as reaction (7) produces a mole of CO₂ per mole of CO, the rate of CO in the hot zone ($\dot{n}'_{\text{CO}}|_{\text{O}_2}$) may be bounded as

$$\dot{n}'_{\text{CO}}(t)|_{\text{O}_2} \leq \dot{n}'_{\text{CO}}(t)|_{\text{O}_2} \leq [\dot{n}'_{\text{CO}}(t) + \dot{n}'_{\text{CO}_2}(t)]|_{\text{O}_2} \quad (27)$$

Owing to the high dilution of the product gas with Ar ($y_{\text{Ar}}(t) \approx 0.9$ – 0.95) the total molar rate was not significantly different between the hot zone and the outlet, *i.e.* $\dot{n}'(t) \approx \dot{n}(t)$, which results in $\tilde{y}'(t) \approx \tilde{y}(t)$. Therefore, the partial pressure of CO in the hot zone is estimated as

$$[\tilde{y}_{\text{CO}}(t)\tilde{p}'_{\text{tot}}(t)]|_{\text{O}_2} \leq \tilde{p}'_{\text{CO}}(t)|_{\text{O}_2} \leq [(\tilde{y}_{\text{CO}}(t) + \tilde{y}_{\text{CO}_2}(t))\tilde{p}'_{\text{tot}}(t)]|_{\text{O}_2} \quad (28)$$

3.5.2 Selecting the initial amounts of C and partial pressures of CO in the sweep for the reference CTR experiments.

As already discussed in section 2.2, the initial amounts of C for the reference CTR experiments performed in phase 3 of the experimental program were selected according to eqns (18) and (19). It should be noted that eqns (18) and (19) account for the consumption of C not only from the reactant blend but also from both the extra layer of C and the graphite felt, thereby making the effective C/MgO ratios in the reference CTR experiments lower than their counterparts in the comparison runs of experimental phases 1 and 2. This could only have an adverse effect on the extent of CTR in the reference experiments. Therefore, if the CTR extents in the reference experiments are still higher than the CTR extents resulting from those of the comparison runs then the discrimination of the reaction pathway becomes only more conservative.

The composition and the flow rate of the CO–Ar sweep in the reference CTR experiments was selected such that the resulting p'_{CO} observed in the absence of CTR matched the highest CO partial pressures observed during the C oxidation experiments performed under O₂–Ar and CO₂–Ar sweeps in the absence of MgO.

3.5.3 The extents of CTR. In the absence of O₂ or CO₂ in the feed, the extent of CTR was calculated from the MgO bal-

ance in the hot zone as

$$\xi_1 = N_{\text{MgO}}^0 - N_{\text{MgO}}^f = \frac{m_{\text{MgO}}^0 - m_{\text{MgO}}^f}{M_{\text{MgO}}}, \quad (29)$$

where m_{MgO}^f is the mass of the unreacted MgO in the residual reactant blend that was determined by thermogravimetry, as described in section S4 of the ESI.†

The presence of O₂ or CO₂ in the sweep gas, however, precludes direct calculation of ξ_1 *via* eqn (29) as some of the produced Mg_(g) may re-oxidize within the hot zone *via* reverse reactions (2) and (4) to the extent that is not known. For this reason, the extents of CTR for the comparison runs of phases 1 and 2 were estimated exploiting the overall C balance and assuming that the amount of C removed by the CTR is approximately equal to the amount of the reduced MgO, as suggested by the overall reaction (1). Based on the reactions listed in Table 4, this amount of C corresponds to the molar extent of reaction (1) expressed as

$$\xi_1|_{\tau_f} = \underbrace{[N_{\text{CO}}(\tau_f) + N_{\text{CO}_2}(\tau_f)]}_{\text{amount of C entrained by the product gas}} - \underbrace{N_{\text{C, fed}}(\tau_f)}_{\text{amount of C fed with the sweep gas}} - \underbrace{[N_{\text{C}}^0 - \tilde{N}_{\text{C}}(\tau_f)]}_{\text{amount of C consumed by the oxidant in the sweep}} + \underbrace{N_{\text{C, dep}}(\tau_f)}_{\text{amount of C deposited in the cooling zone}} \quad (30)$$

with the individual terms defined as follows:

$$N_{\text{C, fed}}(\tau_f) = \left\{ \begin{array}{l} 0|_{\text{O}_2} \\ [N_{\text{CO}_2, \text{ fed}}(\tau_f)]|_{\text{CO}_2} \end{array} \right\}, \quad (31)$$

$$N_{\text{C}}^0 - \tilde{N}_{\text{C}}(\tau_f) = \left\{ \left[\xi_5(\tau_f) + \xi_6(\tau_f) \right]|_{\text{O}_2}, \left[\xi_5(\tau_f) \right]|_{\text{CO}_2} \right\}, \quad (32)$$

$$N_{\text{C, dep}}(\tau_f) = \left\{ \left[\varphi_1^*(\tau_f) + \varphi_5^*(\tau_f) \right]|_{\text{O}_2}, \left[\varphi_1^*(\tau_f) + \varphi_5^*(\tau_f) \right]|_{\text{CO}_2} \right\} \quad (33)$$

The total amount of fed CO₂ was determined as

$$N_{\text{CO}_2, \text{ fed}}(\tau_f) = y_{\text{CO}_2}^0 \int_{\tau_{\text{ox}}}^{\tau_f} \dot{n}^0(t) dt \quad (34)$$

where $y_{\text{CO}_2}^0$ represents the mole fraction of CO₂ in the inlet sweep gas mixture. However, if either O₂ or CO₂ is present in the sweep gas, the five reaction extents listed in Table 4 cannot be calculated based on the measured CO and CO₂ outlet mole rates as the only information available. While the need



Table 4 Reactions involving C during the CTR experiments. Note: the extents $\varphi_1^* \geq 0$ and $\varphi_5^* \geq 0$ refer to the extents of the reverse reactions (1) and (5).

Amounts of C	Reactions		Phase 1:	Phase 2:	Phase 3:
	Extent	Stoichiometry	O ₂ -Ar	CO ₂ -Ar	CO-Ar, Ar
Consumed by the CTR	ξ_1	$\text{MgO}_{(s)} + \text{C}_{(s)} \rightleftharpoons \text{Mg}_{(g)} + \text{CO}_{(g)}$	✓	✓	✓
Hot zone Consumed by the oxidant added to the sweep	ξ_6	$\text{C}_{(s)} + \text{O}_{2(g)} \rightleftharpoons \text{CO}_{2(g)}$	✓	✗	✗
	ξ_5	$\text{C}_{(s)} + \text{CO}_{2(g)} \rightleftharpoons 2\text{CO}_{(g)}$	✓	✓	✗
Cooling zone Deposited on the column wall	φ_1^*	$\text{Mg}_{(g/l/s)} + \text{CO}_{(g)} \rightleftharpoons \text{MgO}_{(s)} + \text{C}_{(s)}$	✓	✓	✓
	φ_5^*	$2\text{CO}_{(g)} \rightleftharpoons \text{C}_{(s)} + \text{CO}_{2(g)}$	✓	✓	✓

for extents ξ_5 and ξ_6 can be conveniently circumvented by calculating the final amount of C in the absence of CTR $\tilde{N}_C(\tau_f)$ according to eqns (18) and (19), respectively, the final amount of deposited C $N_{C,\text{dep}}(\tau_f)$ ranging as

$$0 \leq N_{C,\text{dep}}(\tau_f) \leq [\varphi_1^*(\tau_f) + \varphi_5^*(\tau_f)] \quad (35)$$

cannot be calculated. However, this amount can be readily calculated for the reference CTR experiments performed under Ar or an Ar-CO sweep for which the extent of CTR ξ_1 is determined *via* the MgO balance eqn (29). As in this case $\xi_5 = \xi_6 = 0$ and

$$N_{C,\text{fed}}(\tau_f) = N_{\text{CO, fed}}(\tau_f) = y_{\text{CO}}^0 \int_{\tau_{\text{ox}}}^{\tau_f} \dot{n}^0(t) dt, \quad (36)$$

eqns (30), (32), (33), and (36) imply that

$$\begin{aligned} N_{C,\text{dep}}(\tau_f)|_{\text{ref}} &= [\varphi_1^*(\tau_f) + \varphi_5^*(\tau_f)]|_{\text{ref}} \\ &= [N_{\text{CO, fed}}(\tau_f) + \xi_1(\tau_f) - N_{\text{CO}}(\tau_f) - N_{\text{CO}_2}(\tau_f)]|_{\text{ref}}. \end{aligned} \quad (37)$$

As the amount of C deposited in the cooling zone increases with the increase in the partial pressures of Mg and CO, one of the reference experiments should be performed under conditions ensuring the highest $[\varphi_1^*(\tau_f) + \varphi_5^*(\tau_f)]|_{\text{ref}}$ within the range of the conditions investigated. Using this value as the estimate of the higher limit for the amount of C deposited during the comparison runs of phases 1 and 2 will only inflate the extents of the CTR in those runs. Since the CTR mechanism can be discriminated if one of the CTR extents from the comparison runs is lower than the lowest CTR extent observed in the reference experiments of phase 3, this approach should make the decision only more conservative.

4 Results and discussion

4.1 Phase 1: O₂-Ar sweep

4.1.1 Detection of the onset of CTR. Table 5 summarizes the initial conditions selected for the tests under an O₂-Ar sweep. These conditions were implemented at three furnace setpoint temperatures (T_{sp}): 1375, 1400, and 1450 °C. Fig. 4 shows a comparison of the outlet CO, CO₂, and O₂ molar flow rates in the product gas from the experiments with the MgO-C and Al₂O₃-C blends at 1375 °C; the results for the remaining two setpoint temperatures are shown in section S5 of the ESI.† The onset of the CTR was identified at $\tau_1 \approx 22$ min by the inflection point of the CO molar rate observed with the MgO-C blend. The amount of Al₂O₃ for the Al₂O₃-C blend (20.1 mmol) was selected to match the heat capacity of the substituted MgO, thereby providing an equal sink for the heat released by the exothermic reaction (3). This resulted in a good agreement between the CO production rates with these two blends prior to the onset of CTR. This agreement could not be achieved with C alone (see Fig. S2 of section S5 of the ESI†) which has been attributed to the increase in the local temperature of the C bed due to exothermic reaction (3) ($\Delta h^0 = -110.5$ kJ mol⁻¹ (ref. 24)). The CO₂ observed in the outlet was attributed to reaction (6) taking place in the hot zone and/or reaction (7) taking place in the hot and/or cooling zone. Lower CO₂ and O₂ product flows in the test with MgO-C compared to those observed with Al₂O₃-C implied the re-oxidation of (i) Mg_(g/l/s) *via* reverse reactions (2) and (4) taking place in the hot and/or cooling zone and (ii) deposited C *via* reactions (3) and (6) taking place in the cooling zone only.

4.1.2 Quantifying the amount of C removed by co-fed O₂. Following the procedure outlined in section 3.5.1, the amounts of C at the onset of CTR were found to be $\tilde{N}_C(\tau_1)|_{\text{O}_2} = 47.1 \pm 0.15$ mmol over the entire temperature range investigated. The final amount of C in the absence of

Table 5 The initial conditions for the tests under an O₂-Ar sweep (phase 1 of the experimental program).

Sweep gas	\dot{V}_N (L _N min ⁻¹)	p_{O_2} in the sweep (Pa)	Solids	N_{MgO}^0 (mmol)	$N_{\text{Al}_2\text{O}_3}^0$ (mmol)	N_C^0 (mmol)	N_C^0/N_{MgO}^0 (—)
5% O ₂ -Ar	0.160	40	C	—	—	53.3	—
5% O ₂ -Ar	0.160	40	Al ₂ O ₃ -C	—	20.1	53.3	—
5% O ₂ -Ar	0.160	40	MgO-C	49.6	—	53.3	1.08



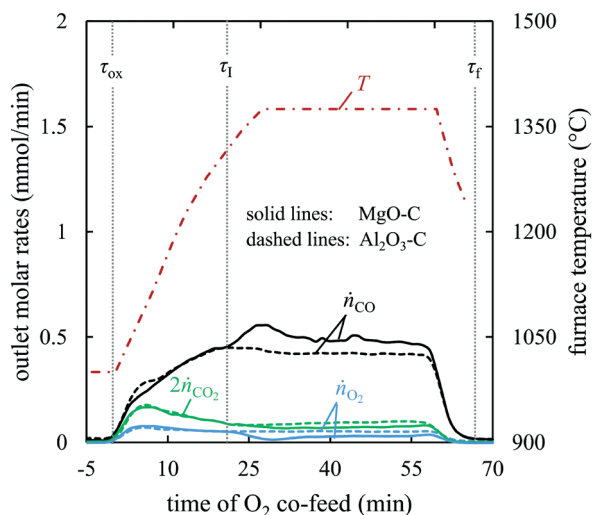


Fig. 4 Outlet molar rates of CO, CO₂, and O₂ for MgO–C and Al₂O₃–C blends subjected to an O₂–Ar sweep at $T_{sp} = 1375$ °C. Note: the mole rate of CO₂ is shown doubled to ease visual distinction from the mole rate of O₂.

CTR $\tilde{N}_C(\tau_1)|_{O_2}$ decreased from 31.6 at 1375 °C to 26.6 mmol at 1450 °C. This decrease was attributed mainly to the increase in the durations of the heating and cooling temperature ramps that increased the total duration of O₂ co-feed from 60 min at $T_{sp} = 1375$ °C to 73 min at $T_{sp} = 1450$ °C. At the same time, the C consumption in the experiments with the Al₂O₃–C blend was essentially unaffected by an increase in T_{sp} (see section S5 of the ESI†). This, together with a roughly constant CO production rate once the temperature stabilized at T_{sp} , confirms that the oxidation of C in these experiments was controlled by film diffusion which for the typical C conversion of 12–17% implies an essentially constant conversion rate.²⁵ With the total $p'_{tot}|_{O_2} \sim 0.8$ kPa, $p'_{CO}|_{O_2}$ was in the range 55–65 Pa and 60–75 Pa at 1375 °C and 1450 °C, respectively.

4.2 Phase 2: CO₂–Ar sweep

4.2.1 Detection of the onset of CTR. Table 6 summarizes the initial conditions selected for the tests under a CO₂–Ar sweep. These conditions were implemented at three furnace setpoint temperatures (T_{sp}): 1375, 1400, and 1450 °C. Fig. 5 shows a comparison of the outlet CO, CO₂, and O₂ molar flow rates in the product gas from the experiments with the MgO–C blend and C alone at 1375 °C; the results for the

remaining two setpoint temperatures are shown in section S5 of the ESI† and the repeatability of the experiments is demonstrated in section S6 of the ESI†. The onset point of CTR was identified at $\tau_1 \approx 22$ min as the time stamp of the inflection point of the CO molar flow rate obtained with the MgO–C blend. Markedly, good agreement between the data sets for $t < \tau_1$ was achieved even without diluting C with Al₂O₃. This was attributed to the endothermic consumption of C by CO₂ *via* reaction (5) ($\Delta h^0 = +172.4$ kJ mol⁻¹ (ref. 24)). As was the case for the O₂–Ar sweep, once the temperature stabilized at T_{sp} the production of CO due to the consumption of C with co-fed CO₂ was approximately constant and essentially independent of T_{sp} (see section S5 of the ESI†). A decrease in the molar rate of CO₂ observed with the C–MgO during CTR compared to that observed during C oxidation experiments with C alone was attributed to the oxidation of Mg(g/l/s) and *via* reverse reaction (4) taking place in the hot and/or cooling zone.

4.2.2 Quantifying the amount of C removed by co-fed CO₂.

Following the procedure outlined in section 3.5.1, the amounts of C at the onset of CTR were found to be $\tilde{N}_C(\tau_1)|_{CO_2} = 47.8 \pm 0.05$ mmol over the entire temperature range investigated. As was the case for the tests under an O₂–Ar sweep, the final amount of C in the absence of CTR $\tilde{N}_C(\tau_f)|_{CO_2}$ decreased with increasing T_{sp} from 32.6 mmol at 1375 °C to 31.8 and 27.5 mmol at 1400 °C and 1450 °C, respectively, mainly because of the prolonged duration of the CO₂ co-feed. Compared to the O₂–Ar sweep experiments, the relative differences between the calculated values of $\tilde{N}_C(\tau_1)$ and of $\tilde{N}_C(\tau_f)$ were $\leq 2\%$ and $\leq 4\%$, respectively (see section S7 of the ESI†). The set of conditions listed in Table 6 therefore provided that $\tilde{N}_C(\tau_1)|_{CO_2} \approx \tilde{N}_C(\tau_1)|_{O_2}$ and $\tilde{N}_C(\tau_f)|_{CO_2} \approx \tilde{N}_C(\tau_f)|_{O_2}$ (see eqn (8)) thus no iterations with different CO₂–Ar sweep flow rates and/or compositions mentioned in section 2.2 and Table S1 of section S2 in the ESI† were needed. With $p'_{tot}|_{CO_2} \sim 1.5$ kPa, $\tilde{p}'_{CO_2}|_{CO_2}$ was approximately constant at T_{sp} and ranged from 94 Pa ($T_{sp} = 1375$ °C) to 97 Pa ($T_{sp} = 1450$ °C) (see section S7 of the ESI†).

4.3 Phase 3: Ar and CO–Ar sweeps

The initial conditions selected for the reference CTR experiments under CO–Ar and Ar sweeps are shown in Table 7. The starting amounts of C for the blends with N_{MgO}^0 moles of MgO were selected to satisfy $N_C^0|_{high} \approx \tilde{N}_C(\tau_1)$ and $N_C^0|_{low} \approx \tilde{N}_C(\tau_f)$. To account for the observed decrease in $\tilde{N}_C(\tau_f)$ with an increase in T_{sp} , $N_C^0|_{low}$ was adjusted to 32.9,

Table 6 The initial conditions for the tests under a CO₂–Ar sweep (phase 2 of the experimental program).

Sweep gas	\dot{V}_N (L _N min ⁻¹)	p_{CO_2} in the sweep (Pa)	Solids	N_{MgO}^0 (mmol)	N_C^0 (mmol)	N_C^0/N_{MgO}^0 (—)
5% CO ₂ –Ar	0.310	75	C	—	53.3	—
5% CO ₂ –Ar	0.310	75	MgO–C	49.6	53.3	1.08



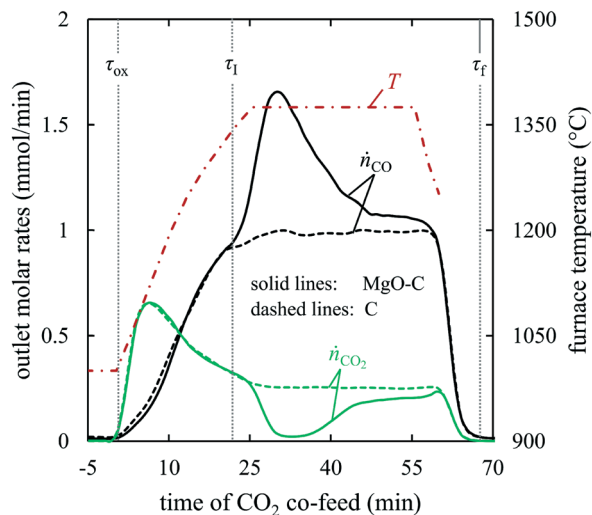


Fig. 5 Outlet molar rates of CO and CO₂ for MgO-C and C alone subjected to the CO₂-Ar sweep at $T_{Sp} = 1375$ °C.

31.6, and 26.6 mmol for $T_{Sp} = 1375$, 1400, and 1450 °C, respectively. The higher limit of CO partial pressure in the sweep was set to $p_{CO} = 95$ Pa to match $\bar{p}'_{CO}|_{CO_2}$ that ranged from 94 to 97 Pa. This was accomplished by flowing a 5% CO-Ar mixture with a normal flow rate $\dot{V}'_N = 0.39$ L_N min⁻¹, which resulted in $p'_{tot} \approx 1.9$ kPa. The total normal flow rate of the Ar sweep was chosen to be the same as that of the CO-Ar sweep (0.39 L_N min⁻¹) also resulting in $p'_{tot} \approx 1.9$ kPa.

The outlet gas in all the reference experiments comprised only Ar and CO. Fig. 6 indicates a remarkable similarity between the outlet CO molar rates observed during the comparison experiments under the CO₂-Ar sweep and the reference experiments under the CO-Ar sweep with $N_C^0|_{high}$. As expected, the outlet CO molar rates observed under the O₂-Ar sweep were lower. The results of the experiments performed under the Ar sweep with $N_C^0|_{high}$ and the CO-Ar sweep with $N_C^0|_{low}$ are also available in section S5 of the ESI†

In spite of the absence of CO₂ in the outlet gas during the experiments completed under CO-Ar and Ar sweeps, visual

inspection of the cooling zone upon these experiments confirmed the presence of deposited C, MgO and/or Mg. This implies that C may have deposited as a consequence of the direct recombination of the products *via* the reverse reaction (1). The other possibility is that the condensed Mg_(l/s) may have catalyzed the Boudouard reaction (as C deposition was not observed at up to $p_{CO} \leq 95$ Pa in the absence of CTR) but that the produced CO₂ was completely consumed by the Mg_(g/l/s) reoxidation *via* the reverse reaction (4). This scenario would impose the equality of the extents of the reverse reactions (4) and (5), *i.e.* $\varphi_4^* = \varphi_5^*$, thereby making the Boudouard reaction only a step of the reverse overall reaction (1), as suggested by Hischier *et al.*¹⁵

4.4 Discrimination of the prevailing reaction pathways

The extents of CTR calculated as outlined in section 3.5.3 are normalized by $N_{MgO}^0 = 49.6$ mmol and shown in Fig. 7 as a function of T_{Sp} . The highest amount of C deposited in the cooling zone, indicating the highest φ_1^* and φ_5^* , is expected to be observed in the experiment performed with the higher initial amount of C $N_C^0|_{high} = 47.5$ mmol under the CO-Ar sweep as this experiment resulted in the highest Mg_(g) production and the highest p_{CO} in the cooling zone. Therefore, setting the maximum amount of deposited C to the amount calculated for this particular experiment, *i.e.*,

$$\max[\varphi_1^*(\tau_f) + \varphi_5^*(\tau_f)] = [\varphi_1^*(\tau_f) + \varphi_5^*(\tau_f)]|_{CO, N_C^0|_{high}} \quad (38)$$

allows for bounding the extents of CTR calculated for the comparison runs *via* eqn (30) by the error bars reflecting the uncertainty of $N_{C,dep}(\tau_f)$ as

$$0 \leq N_{C,dep}(\tau_f) \leq [\varphi_1^*(\tau_f) + \varphi_5^*(\tau_f)]|_{CO, N_C^0|_{high}} \quad (39)$$

The results presented in Fig. 7 can be summarized as follows:

(A) The addition of CO to the sweep gas slightly suppresses the Mg_(g) production (data set II *versus* data set I);

Table 7 The initial conditions for the reference tests completed under a CO-Ar or Ar sweep (phase 3 of the experimental program).

T_{Sp} (°C)	Sweep gas	\dot{V}'_N (L _N min ⁻¹)	p_{CO} in the sweep (Pa)	Solids	N_{MgO}^0 (mmol)	$N_C^0 _{high}$ (mmol)	$N_C^0 _{low}$ (mmol)	N_C^0/N_{MgO}^0 (—)
1375	5% CO-Ar	0.390	95	MgO-C	49.6	47.5	—	0.96
	5% CO-Ar	0.390	95	MgO-C	49.6	—	32.9	0.67
	Ar	0.390	—	MgO-C	49.6	47.5	—	0.96
1400	5% CO-Ar	0.390	95	MgO-C	49.6	47.5	—	0.96
	5% CO-Ar	0.390	95	MgO-C	49.6	—	31.6	0.64
	Ar	0.390	—	MgO-C	49.6	47.5	—	0.96
1450	5% CO-Ar	0.390	95	MgO-C	49.6	47.5	—	0.96
	5% CO-Ar	0.390	95	MgO-C	49.6	—	26.6	0.54
	Ar	0.390	—	MgO-C	49.6	47.5	—	0.96



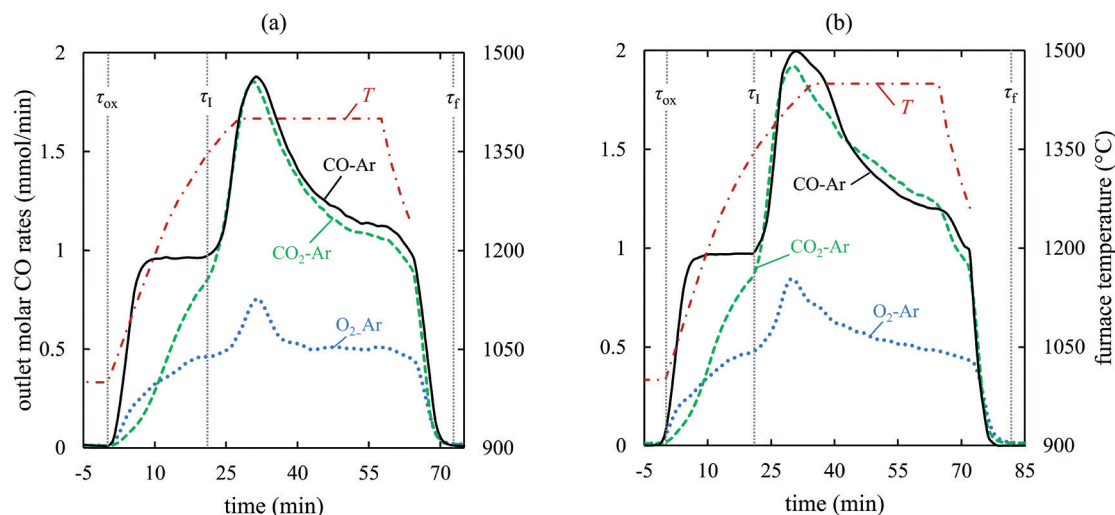


Fig. 6 CO molar rates observed at (a) $T_{\text{SP}} = 1400$ °C and (b) 1450 °C with $N_{\text{C}}^0|_{\text{high}} \approx \tilde{N}_{\text{C}}(\tau_1) \approx \tilde{N}_{\text{C}}(\tau_1) = 47.5$ mmol and $N_{\text{MgO}}^0 = 49.6$ mmol under CO-Ar (black solid line), CO₂-Ar (green dashed line) and O₂-Ar (blue dotted line). A comparison of the CO molar rates for 1375 °C is shown in section S5 of the ESI†

therefore, the runs performed under the CO-Ar sweep (data sets II and IV) may serve as a conservative reference for the CTR in the absence of the oxidants in the sweep.

(B) The extents of CTR in the comparison experiments performed under the O₂-Ar sweep with $N_{\text{C}}^0|_{\text{high}}$ (data set V)

were up to 60% lower than those obtained under the CO-Ar sweep with $N_{\text{C}}^0|_{\text{low}}$ (data set IV).

(C) The extents of CTR in the comparison experiments performed under the CO₂-Ar sweep with $N_{\text{C}}^0|_{\text{high}}$ (data set III) were lower than those obtained under the CO-Ar sweep with $N_{\text{C}}^0|_{\text{high}}$ (data set II) but higher than those obtained under the CO-Ar sweep with $N_{\text{C}}^0|_{\text{low}}$ (data set IV).

As the addition of O₂ to the sweep showed no facilitating effect on the sintering of MgO (see Fig. S13 in section S8 of the ESI†), the O₂-induced suppression of the Mg_(g) production in spite of a more favorable C/MgO ratio (observation B) can be attributed only to the equilibrium shifts of reactions (2) and/or (4) because of the potential increase in both p'_{O_2} and the ratio $p'_{\text{CO}_2}/p'_{\text{CO}}$. The former can be estimated from the outlet O₂ molar rates and then used to calculate the equilibrium partial pressures of Mg resulting from the MgO dissociation (reaction (2)) according to the analysis presented in section S10 of the ESI†. These equilibrium partial pressures were five to six orders of magnitude lower than the partial pressures of Mg estimated from the observed Mg_(g) productions, as described in section S9 of the ESI†. This implies that at T_{SP} values of 1375 °C and 1400 °C the MgO dissociation (reaction (2)) essentially did not contribute to the Mg_(g) production under the O₂-Ar sweep (data set V). It should be noted that this claim cannot be extended to the experiment performed at $T_{\text{SP}} = 1450$ °C as the outlet O₂ molar rate was essentially zero during a part of this experiment, hence the thermal dissociation could have taken place also. Using analogous reasoning outlined in S10 of the ESI† to estimate $p'_{\text{CO}_2}/p'_{\text{CO}}$ ratios for the experiments under the CO₂-Ar sweep (data set III) indicates that the partial pressures of Mg estimated from the observed Mg_(g) productions are ~20 to 4000 times higher than those predicted by the equilibrium of reaction (4). This implies that under the CO₂-Ar sweep (data set III) the MgO reduction with CO (reaction (4)) essentially did not contribute to the Mg_(g) production.

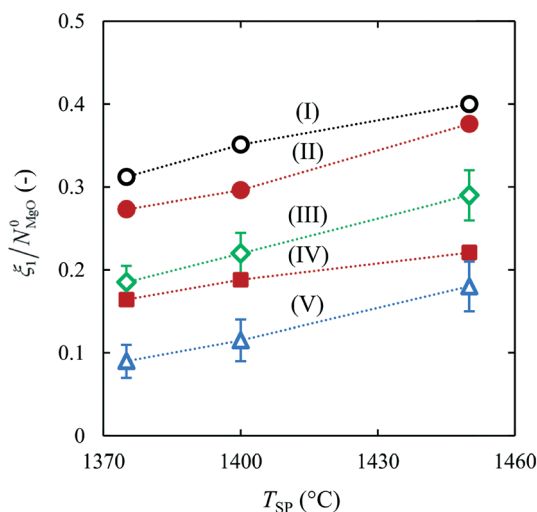


Fig. 7 Normalized extents of CTR as a function of T_{SP} under (I) an Ar sweep with $N_{\text{C}}^0 = N_{\text{C}}^0|_{\text{high}} = 47.5$ mmol (open circles), (II) a CO-Ar sweep with $N_{\text{C}}^0 = N_{\text{C}}^0|_{\text{high}} = 47.5$ mmol (filled circles), (III) a CO₂-Ar sweep with $N_{\text{C}}^0 = 53.3$ mmol corresponding to $\tilde{N}_{\text{C}}(\tau_1) = 47.8$ mmol $\approx N_{\text{C}}^0|_{\text{high}}$ (open diamonds), (IV) a CO-Ar sweep with $N_{\text{C}}^0 = N_{\text{C}}^0|_{\text{low}} = 32.9$ (1375 °C), 31.6 (1400 °C), and 26.6 mmol (1450 °C) (filled squares) and (V) an O₂-Ar sweep with $N_{\text{C}}^0 = 53.3$ mmol corresponding to $\tilde{N}_{\text{C}}(\tau_1) = 47.1$ mmol $\approx N_{\text{C}}^0|_{\text{high}}$ (open triangles). The error bars for the comparison runs (III and V) represent $[\phi_1^*(\tau_f) + \phi_2^*(\tau_f)]$ calculated via eqn (37) for the experiments from the set (II) as the expected maximum of $\tilde{N}_{\text{C,dep}}(\tau_f)$. The dotted lines are added only to indicate trends.



A plausible explanation for the observed O₂ and CO₂ effects is that Mg_(g) is produced *via* both (a) MgO thermal dissociation and (b) MgO reduction with CO that take place in parallel. The role of C is to remove the intermediates O₂ and CO₂ from the reaction sites, thereby favoring forward reactions (2) and (4). Markedly, at 1375 °C and 1400 °C the sums of the extents obtained under the CO₂-Ar (data set III) and O₂-Ar sweeps (data set V) are essentially equal to the extents obtained under the Ar-CO sweep (data set II) (see Fig. S14, section S11 of the ESI†); at 1450 °C, the sum slightly exceeds the extent from the data set II which could be attributed to the Mg_(g) production under the O₂-Ar sweep partly to the MgO dissociation also. This implies that adding O₂ or CO₂ to the sweep allows the isolation of one of the steps by preventing the other and to determine that at 1375 °C and 1400 °C roughly twice as much Mg_(g) was produced *via* the MgO dissociation compared to the MgO reduction with CO.

The conclusion outlined above appears to contradict the claim by Chubukov *et al.*¹⁴ who have advocated that under the same reaction conditions MgO_(s)-C_(s) boundary reaction governs the Mg_(g) production rather than MgO dissociation. It should be noted that the disagreement may be existing only in the interpretation of the same reaction mechanism. Specifically, the MgO dissociation (reaction (2)) is sustained by the removal of O₂ from the MgO surface *via* oxidation of C (reaction (3)) and the sum of these two steps results in the stoichiometry of the overall reaction (1). However, there is no evidence supporting the relevance of a direct solid-solid reaction. In fact, the results of the comparison experiments presented in Fig. 7 indirectly demonstrate that the contact between the materials is not a factor. In particular, the CTR experiments under the O₂-Ar and the CO₂-Ar sweeps (data sets III and V, respectively) were performed with the same initial amount of C which was pre-oxidized to essentially the same extent before reaching the onset temperature of CTR (see Fig. S10 of section S7 in the ESI†). Therefore, the pre-oxidation of C with O₂ and CO₂ should have affected the interfacial contact between the materials in the same way. Yet, the extents of the MgO reduction under the CO₂-Ar sweep are roughly twice as high compared to those observed under the O₂-Ar sweep.

5 Summary and conclusions

This work discriminates the prevailing reaction pathways of the carbothermic reduction of MgO for normalized reduction extents of up to 0.4 achieved within the temperature and pressure ranges of 1375–1450 °C and 1–2 kPa, respectively. It demonstrates that Mg_(g) is produced in the ratio ~2:1 *via* (1) MgO thermal dissociation and (2) MgO reduction with CO that take place in parallel. These pathways generate O₂ (pathway 1) and CO₂ (pathway 2) as the intermediates that diffuse and react with C, thereby sustaining the Mg production. It is also argued that the MgO dissociation pathway may have been confused with

the MgO_(s)-C_(s) boundary reaction advocated by previous investigators, which relies on the direct contact of the solid reactants. Therefore, our findings imply that the rate of the overall MgO reduction may be controlled by the diffusion of the intermediates from the MgO_(s) surface to the C_(s) surface and/or a loss of the MgO surface area due to sintering rather than by the loss of the direct contact between MgO_(s) and C_(s).

Nomenclature

\bar{d}	Volume-based mean particle size (μm)
Δh^0	Standard molar enthalpy of reaction (kJ mol ⁻¹)
K_i	Equilibrium constant of reaction <i>i</i>
l	Length (mm)
m_j^0	Initial mass of species, as-received material, or sample <i>j</i> (g)
m_j^f	Final mass of species, as-received material, or sample <i>j</i> (g)
m_C^*	Mass of extra C layer on top of the felt (g)
M_j	Molar mass of species <i>j</i> (g mmol ⁻¹)
N_j^0	Initial molar amount of species <i>j</i> (mmol)
$N_j(t)$	Temporal molar amount of species <i>j</i> (mmol)
$\tilde{N}_j(t)$	Temporal molar amount of species <i>j</i> in the absence of CTR (mmol)
$N_{C,dep}(\tau)$	Molar amount of C deposited as solid in the cooling zone at time τ (mmol)
$N_{j,fed}(\tau)$	Molar amount of species <i>j</i> co-fed with the sweep up to time τ (mmol)
N_{MgO}^f	Final molar amount of residual MgO after the experiment (mmol)
$\dot{n}_j^0(t)$	Temporal molar flow rate of species <i>j</i> at the inlet (mmol min ⁻¹)
$\dot{n}_j'(t)$	Temporal molar flow rate of species <i>j</i> in the hot zone (mmol min ⁻¹)
$\dot{n}_j(t)$	Temporal molar flow rate of species <i>j</i> at the outlet (mmol min ⁻¹)
$\tilde{\dot{n}}_j(t)$	Temporal molar flow rate of species <i>j</i> in the absence of CTR (mmol min ⁻¹)
$\bar{\dot{n}}_j(t)$	Average molar flow rate of species <i>j</i> (mmol min ⁻¹)
$\dot{n}_{C,dep}(t)$	Rate of C depositing as solid in the cooling zone (mmol min ⁻¹)
p_j'	Partial pressure of species <i>j</i> in the hot zone (Pa)
\tilde{p}_j'	Partial pressure of species <i>j</i> in the hot zone in the absence of CTR (Pa)
\bar{p}_j'	Average partial pressure of species <i>j</i> in the hot zone (Pa)
$p_{Mg,eq}'$	Equilibrium partial pressure of Mg in the hot zone (Pa)
T	Temperature (°C)
T_{ox}	Onset temperature of oxidation of C by co-fed oxidants (°C)
T_1	Onset temperature of CTR (°C)
T_{SP}	Setpoint temperature of the furnace (°C)
T_{sint}	Sintering temperature (°C)



t	Time (min)
$\dot{V}_N^0(t)$	Temporal normal volume flow rate at the inlet (L min ⁻¹)
w_i^j	Mass fraction of compound i in the as-received material j (%)
X_{MgO}	Conversion extent of MgO
$y_j^0(t)$	Temporal molar fraction of species j at the inlet
$y_j^*(t)$	Temporal molar fraction of species j in the hot zone
$y_j(t)$	Temporal molar fraction of species j at the outlet
Z	Fraction of CO consumed by Mg in the cooling zone

Greek symbols

ϕ_j	Molar extent of reaction j taking place in the cooling zone (mmol)
ϕ_j^*	Molar extent of reverse reaction j taking place in the cooling zone (mmol)
ξ_i	Molar extent of reaction i taking place in the hot zone (mmol)
ξ_i^*	Molar extent of reverse reaction i taking place in the hot zone (mmol)
τ_{ox}	Onset point of oxidation of C by co-fed oxidants (min)
τ_I	Onset point of CTR (min)
τ_{II}	End point of CTR (min)
τ_f	Final point of test (min)

Subscripts

imp	Impurity
N	Normal (0 °C and 101.3 kPa)
tot	Total
vm	Volatile matter
$ _{\text{O}_2}$	O ₂ -Ar sweep
$ _{\text{CO}_2}$	CO ₂ -Ar sweep
$ _{\text{int}}$	Intermediate (O ₂ -Ar sweep or CO ₂ -Ar sweep)
$ _{\text{high}}$	High initial amount of C
$ _{\text{low}}$	Low initial amount of C

Abbreviations

CTR	Carbothermic reduction
MFC	Mass flow controller
SSA	Specific surface area

Conflicts of interest

There are no conflicts to declare.

Acknowledgements

The authors are grateful to Professor Aldo Steinfeld for providing financial support and allowing the use of the facilities and resources within the Professorship for Renewable Energy Carriers at ETH Zürich and to Simon Ackermann, Brendan Bulfin, Christopher Muhich, Michael Takacs, David Weibel, and Vladimir Paunovic for fruitful discussions.

References

- 1 F. Cherubini, M. Raugi and S. Ulgiati, *Resour., Conserv. Recycl.*, 2008, **52**, 1093–1100.
- 2 S. Das, *JOM*, 2008, **60**, 63–69.
- 3 J. Du, W. Han and Y. Peng, *J. Cleaner Prod.*, 2010, **18**, 112–119.
- 4 F. Gao, Z. Nie, Z. Wang, X. Gong and T. Zuo, *Int. J. Life Cycle Assess.*, 2009, **14**, 480–489.
- 5 S. Ehrenberger, H. Dieringa and H. Friedrich, *Life Cycle Assessment of Magnesium Components in Vehicle Construction*, I. o. V. Concepts, German Aerospace Center DLR, Stuttgart, Germany, 2013.
- 6 *Environmental Profile Report for the European Aluminium Industry - Reference Year 2010*, European Aluminum Association, Brussels, 2013.
- 7 A. Tharumarajah and P. Koltun, *J. Cleaner Prod.*, 2007, **15**, 1007–1013.
- 8 G. Brooks, S. Trang, P. Witt, M. N. H. Khan and M. Nagle, *JOM*, 2006, **58**, 51–55.
- 9 I. Vishnevetsky and M. Epstein, *Sol. Energy*, 2015, **111**, 236–251.
- 10 M. E. Gálvez, A. Frei, G. Albisetti, G. Lunardi and A. Steinfeld, *Int. J. Hydrogen Energy*, 2008, **33**, 2880–2890.
- 11 L. Hong, H. Y. Sohn and M. Sano, *Scand. J. Metall.*, 2003, **32**, 171–176.
- 12 M. Nusheh, H. Yoozbashizadeh, M. Askari, N. Kuwata, J. Kawamura, J. Kano, F. Saito, H. Kobatake and H. Fukuyama, *ISIJ Int.*, 2010, **50**, 668–672.
- 13 M. Halmann, A. Frei and A. Steinfeld, *Miner. Process. Extr. Metall. Rev.*, 2011, **32**, 247–266.
- 14 B. A. Chubukov, A. W. Palumbo, S. C. Rowe, I. Hischier, A. J. Groehn and A. W. Weimer, *Thermochim. Acta*, 2016, **636**, 23–32.
- 15 I. Hischier, B. A. Chubukov, M. A. Wallace, R. P. Fisher, A. W. Palumbo, S. C. Rowe, A. J. Groehn and A. W. Weimer, *Sol. Energy*, 2016, **139**, 389–397.
- 16 K. L. Komarek, A. Coucoulas and N. Klinger, *J. Electrochem. Soc.*, 1963, **110**, 783–791.
- 17 L. Rongti, P. Wei and M. Sano, *Metall. Mater. Trans. B*, 2003, **34**, 433–437.
- 18 Y. Tian, B.-Q. Xu, C.-B. Yang, B. Yang, T. Qu, H.-X. Liu, Y.-N. Dai and D.-C. Liu, *Metall. Mater. Trans. B*, 2014, **45**, 1936–1941.
- 19 G. Levêque and S. Abanades, *Thermochim. Acta*, 2015, **605**, 86–94.
- 20 W.-D. Xie, J. Chen, H. Wang, X. Zhang, X.-D. Peng and Y. Yang, *Rare Met.*, 2016, **35**, 192–197.
- 21 S. Yagi and D. Kunii, *Symp. (Int.) Combust., [Proc.]*, 1955, **5**, 231–244.
- 22 M. Kruesi, M. E. Galvez, M. Halmann and A. Steinfeld, *Metall. Mater. Trans. B*, 2011, **42**, 254–260.
- 23 M. Kogler, E.-M. Köck, B. Klötzer, T. Schachinger, W. Wallisch, R. Henn, C. W. Huck, C. Hejny and S. Penner, *J. Phys. Chem. C Nanomater. Interfaces*, 2016, **120**, 1795–1807.



- 24 A. Roine, *Outokumpu HSC Chemistry for Windows 5.0*, Outokumpu Research Oy, Finland, 2002.
- 25 O. Levenspiel, *Chemical reaction engineering*, John Wiley & Sons, New York, 3rd edn, 1999.

